Vietnam Journal of Science and Technology ***59*** *(6) (2021) 772-785*

doi:10.15625/2525-2518/59/6/15953

FREE VIBRATION ANALYSIS OF CRACKED KIRCHHOFF-LOVE PLATE USING THE EXTENDED RADIAL POINT INTERPOLATION METHOD

Vay Siu Lo*, Nha Thanh Nguyen, Minh Ngoc Nguyen, Thien Tich Truong*

Department of Engineering Mechanics, Faculty of Applied Science, Ho Chi Minh City University of Technology (HCMUT), 268 Ly Thuong Kiet Street, District 10, Ho Chi Minh City, Viet Nam
Vietnam National University Ho Chi Minh City, Linh Trung Ward, Thu Duc District, Ho Chi Minh City, Viet Nam

*Emails: *losiuvay@hcmut.edu.vn, tttruong@hcmut.edu.vn*

Received: 22 March 2021; Accepted for publication: 20 October 2021

Abstract. For plate bending problems, using a plate theory to model thin plate structures is less computationally expensive than 3D modelling. The Kirchhoff-Love plate theory is appropriate for analysing thin plate structures. If the membrane deformation is ignored in the Kirchhoff-Love plate, each node has only one degree of freedom – the deflection. For that reason, the components of the displacement field are calculated only in terms of deflection. This directly reduces the computational cost. However, the Kirchhoff-Love plate requires C^1 continuity and thus leading to complicated mathematical computation in the conventional Finite Element Method (FEM). For this reason, the alternative meshfree method - the Radial Point Interpolation Method (RPIM) is employed in this study. The shape function of the RPIM is formulated from the radial basis and the polynomial basis, so the requirement to calculate the second-order derivative in Kirchhoff-Love theory is easily done. Hence, using the RPIM to model Kirchhoff-Love plate is much easier than FEM. Besides, the analysis of cracked structures is important because it is related to the lifetime of the structures. Therefore, this paper uses the extended radial point interpolation method (XRPIM) to investigate the free vibration of the cracked Kirchhoff-Love plate. The numerical results from this study are compared with those of other researchers to verify the accuracy of the method.

Keywords: fracture, free vibration, Kirchhoff-Love plate, RPIM, XRPIM.

Classification numbers: 5.4.2, 5.4.3, 5.4.6.

1. INTRODUCTION

Thin plate structures are common in practice, so analysis of thin plate is necessary. Furthermore, less number of degree of freedoms (DOFs) is needed in a plate formulation compared to a 3D solid model. Hence, the computational cost is reduced. Besides, fracture analysis is also an important task because it is related to the lifetime of the structures. However, the number of researches on cracked plate is still limited, especially, thin plate using Kirchhoff-

Love theory. Therefore, more investigations on the modelling of cracked thin plates are necessary.

In fracture analysis, a powerful method to model crack discontinuity without remeshing is the eXtened Finite Element Method (XFEM), which was previously proposed [1] and has been widely used. In the XFEM formulation, the discontinuity (jump) in displacement fields and the singularity in stress fields are described using the enrichment functions. The XFEM has been developed for solving thick plates using Reissner-Mindlin theory [2,3,4] and thin plates using Kirchhoff-Love theory [5]. However, in the analysis of Kirchhoff-Love plate, it is necessary to construct a higher-order shape function for the requirement of the second-order derivatives in the Kirchhoff-Love theory [6]. Therefore, it brings computational difficulties.

The Radial Point Interpolation Method (RPIM) [7, 8] is easier to apply the Kirchhoff-Love theory than FEM. In the same manner of formulating XFEM, Nguyen *et al.* introduced XPRIM by combining RPIM and enrichment functions [9, 10, 11], they used this method for 2D fracture analysis. Nevertheless, to the best of our knowledge, fracture analysis in the Kirchhoff-Love plate using XRPIM has not yet been reported. In the scope of this study, only the free vibration behavior of cracked plate is investigated. This paper analyzes the free vibration behavior of thin plates with through-thickness crack. The method used for computing is the XRPIM and using Kirchhoff-Love plate theory for modeling thin plate behavior. The validity of the proposed method is examined through various numerical examples, demonstrating the accuracy of the approach.

2. METHODOLOGY

2.1. Kirchhoff-Love plate theory

Kirchhoff-Love plate theory is used for thin plate problems. The main assumption in this theory is that the cross-section of the plate before and after deformation remains perpendicular to the plate mid surface. Therefore, the shear strain components $\left(\varepsilon_{13}, \varepsilon_{23}\right)$ are zeros [12]. In this study, only one DOF is used, the deflection of the mid surface w. The displacement field of the plate is defined as follows

$$\mathbf{u} = \begin{Bmatrix} u_1 & u_2 & u_3 \end{Bmatrix}^T = \begin{Bmatrix} -x_3 \dfrac{\partial}{\partial x_1} & -x_3 \dfrac{\partial}{\partial x_2} & 1 \end{Bmatrix}^T w \tag{1}$$

where $\dfrac{\partial w}{\partial x_1}$ and $\dfrac{\partial w}{\partial x_2}$ are the rotation about x_1 and x_2 axis, respectively.

From Equation (1) the pseudo-strain is obtained as

$$\varepsilon_p = \begin{Bmatrix} \kappa_{11} & \kappa_{22} & \kappa_{12} \end{Bmatrix}^T = \begin{Bmatrix} -\dfrac{\partial^2 w}{\partial x_1^2} & -\dfrac{\partial^2 w}{\partial x_2^2} & -2\dfrac{\partial^2 w}{\partial x_1 \partial x_2} \end{Bmatrix}^T \tag{2}$$

The relationship between pseudo-strain and pseudo-stress is

$$\sigma_p = \mathbf{D}\varepsilon_p = \begin{Bmatrix} M_1 & M_2 & M_{12} \end{Bmatrix}^T \tag{3}$$

for isotropic homogeneous material, $\mathbf{D}$ is defined as

$$\mathbf{D}=\frac{Et^3}{12\left(1-\nu^2\right)}\begin{bmatrix}1 & \nu & 0\\ \nu & 1 & 0\\ 0 & 0 & \dfrac{(1-\nu)}{2}\end{bmatrix} \tag{4}$$

where E is Young's modulus, t is the thickness of the plate and ν is Poisson ratio.

In discrete form, the deflection of an arbitrary point $\mathbf{x}=\left(x_1,x_2\right)$ on the mid surface is approximated as

$$w^h\left(\mathbf{x}\right)=\sum_I^n \Phi_I\left(\mathbf{x}\right)w_I \tag{5}$$

where Φ_I is RPIM shape functions.

According to the formulation of free vibration in [13], the dynamic equation (without damping) is

$$\mathbf{M}\ddot{\mathbf{w}}+\mathbf{K}\mathbf{w}=0 \tag{6}$$

The stiffness matrix is computed as

$$\mathbf{K}=\int_A \mathbf{B}^T\mathbf{D}\mathbf{B}dA \tag{7}$$

where $\mathbf{B}$ is the column vector containing second order partial derivatives of the shape functions, at I-th node $\mathbf{B}_I$ is a vector including three components

$$\mathbf{B}_I=\left\{-\Phi_{I,11}\quad -\Phi_{I,22}\quad -2\Phi_{I,12}\right\}^T \tag{8}$$

The mass matrix is computed as

$$\mathbf{M}=\int_A \mathbf{N}^T\mathbf{m}\mathbf{N}dA \tag{9}$$

where $\mathbf{N}$ is the column vector containing three components as below

$$\mathbf{N}_I=\left\{\Phi_I\quad \Phi_{I,1}\quad \Phi_{I,2}\right\}^T \tag{10}$$

and $\mathbf{m}$ is the inertia matrix

$$\mathbf{m}=\begin{bmatrix}\rho t & 0 & 0\\ 0 & \dfrac{\rho t^3}{12} & 0\\ 0 & 0 & \dfrac{\rho t^3}{12}\end{bmatrix} \tag{11}$$

ρ is the density.

Equation (6) is now rewritten in the eigenvalue equation form [14] to obtain the solution for the eigenvalue (ω) and eigenvector ($\bar{\mathbf{w}}$).

$$\left(\mathbf{K}-\omega^2\mathbf{M}\right)\bar{\mathbf{w}}=0 \tag{12}$$

2.2. XRPIM

First, a brief explanation of RPIM is presented. The RPIM function Φ_I in this study includes radial basis functions and polynomial basis functions. To avoid the influence of shape parameters, quartic function is used as the radial basis function [15], quartic function is defined as follows

$$R_I(x,y)=1-6\left(\frac{\theta}{l_s}\right)^2 r_I^2+8\left(\frac{\theta}{l_s}\right)^3 r_I^3-3\left(\frac{\theta}{l_s}\right)^4 r_I^4 \tag{13}$$

where θ is the shape parameter, l_s is the length scale parameter and r is the distance between point $\mathbf{x}$ and $\mathbf{x}_I$ and defined as

$$r=\left[\left(x-x_I\right)^2+\left(y-y_I\right)^2\right]^{1/2} \tag{14}$$

The RPIM shape function is defined by $\Phi_I=R_I S_A+p_I S_B$, where p_I denotes the polynomial function, S_A and S_B are the constant matrices. Details on calculation of RPIM shape functions are referred to [8]. The requirement of second-order derivatives in Kirchhoff-Love plate theory is therefore easy to obtain, particularly

$$\begin{aligned}\Phi_{I,11}&=R_{I,11}S_A+p_{I,11}S_B\\ \Phi_{I,22}&=R_{I,22}S_A+p_{I,22}S_B\\ \Phi_{I,12}&=R_{I,12}S_A+p_{I,12}S_B\end{aligned} \tag{15}$$

Meanwhile, the conventional Finite Element Method (FEM) needs to construct higher-order functions [16] to satisfy the requirement for second-order derivatives of the shape functions.

The extended RPIM is based on RPIM with some additional treatments for discontinuity problems. By including enrichment functions, the deflection is now computed as

$$w^h(\mathbf{x})=\sum_{i\in W}\Phi_i(\mathbf{x})w_i+\sum_{j\in W_s}\Phi_j(\mathbf{x})\left(H-H_j\right)w_j^s+\sum_{k\in W_t}\Phi_k(\mathbf{x})\left[\sum_{l=1}^{4}\left(G_l-G_{lk}\right)w_{lk}^t\right] \tag{16}$$

where H is the Heaviside function of point $\mathbf{x}$ and H_j is the Heaviside function of node j-th, the Heaviside function is defined as

$$H\left(f(\mathbf{x})\right)=\begin{cases}1 & if\ \ f(\mathbf{x})>0\\ -1 & if\ \ f(\mathbf{x})<0\end{cases} \tag{17}$$

$f(\mathbf{x})$ is the sign distance function.

The tip enrichment function is defined as follows [12]

$$G_l(r,\theta)=\left\{r^{3/2}\sin\frac{\theta}{2},r^{3/2}\cos\frac{\theta}{2},r^{3/2}\sin\frac{3\theta}{2},r^{3/2}\cos\frac{3\theta}{2}\right\} \tag{18}$$

Equation (16) contains three sets of node. The first one W is the set containing all node in the computational domain. The second one W_s is the set containing the nodes in the support domain split by the crack. And W_t is the set containing the nodes in the support domain that contains the crack tip.

The **B** matrix after applying enrichment function to the Kirchhoff-Love theory is defined as

$$\mathbf{B}_I^{split,enrich} = -\begin{bmatrix} \Phi_{I,11}\left(H-H_I\right) \\ \Phi_{I,22}\left(H-H_I\right) \\ 2\Phi_{I,12}\left(H-H_I\right) \end{bmatrix} \quad \mathbf{B}_I^{tip,enrich} = -\begin{Bmatrix} B_1 & B_2 & 2B_3 \end{Bmatrix}^T \tag{19}$$

where the components of $\mathbf{B}_I^{tip,enrich}$ are

$$\begin{aligned} B_1 &= \Phi_{I,11}\left(G_l - G_{ll}\right) + 2\Phi_{I,1}G_{l,1} + \Phi_I G_{l,11} \\ B_2 &= \Phi_{I,22}\left(G_l - G_{ll}\right) + 2\Phi_{I,2}G_{l,2} + \Phi_I G_{l,22} \\ B_3 &= \Phi_{I,12}\left(G_l - G_{ll}\right) + \Phi_{I,1}G_{l,2} + \Phi_{I,2}G_{l,1} + \Phi_I G_{l,12} \end{aligned} \tag{20}$$

And **N** matrix after applying enrichment functions is defined as below

$$\mathbf{N}_I^{split,enrich} = \begin{bmatrix} \Phi_I\left(H-H_I\right) \\ \Phi_{I,1}\left(H-H_I\right) \\ \Phi_{I,2}\left(H-H_I\right) \end{bmatrix} \quad \mathbf{N}_I^{split,enrich} = \begin{bmatrix} \Phi_I\left(G_l - G_{ll}\right) \\ \Phi_{I,1}\left(G_l - G_{ll}\right) + \Phi_I G_{l,1} \\ \Phi_{I,2}\left(G_l - G_{ll}\right) + \Phi_I G_{l,2} \end{bmatrix} \tag{21}$$

3. RESULTS AND DISCUSSION

3.1. Simply supported plate with a central crack

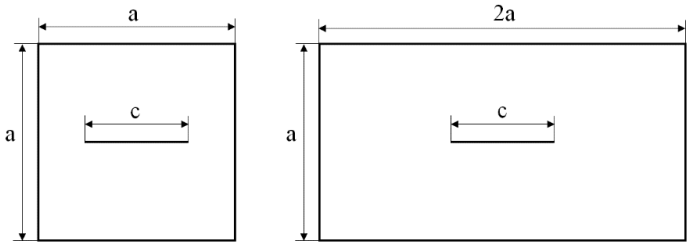

Figure 1. Geometries of a square plate and a rectangular plate containing a central crack.

In this example, two cases of central cracked plate are investigated: a square plate and a rectangular plate. The geometries of two cases are shown in Figure 1. The material properties in this example is Poisson's ratio $\nu = 0.3$. The non-dimensional frequency parameters are computed as $\varpi = \omega a^2\sqrt{\rho t/D}$ and used for comparisons, where $D = Et^3/12\left(1-\nu^2\right)$. In the first case, the ratio of thickness to length $t/a = 0.001$ is used. The plate is discretized into a set of 50×50 nodes. The boundary condition is simply supported in four sides of the square plate (SSSS). Various c/a ratios are considered in this case. Table 1 presents the first five non-dimensional frequencies obtained by other researchers and obtained in this study. The results from XRPIM are in good agreement with other methods. Figure 2 shows the mode shape of five

vibration modes corresponding to the value in Table 1. It is observed that the mode shape of the intact plate is quite similar to the mode shape of the crack plate, except for mode 5. Besides, the crack is not clearly observed in this problem.

Similar to the previous case, a ratio of $t/a = 0.001$ is used to analyze rectangular plate. In this case, the plate is discretized into a set of 80×40 nodes (80 for the long side). The boundary condition is SSSS. Various c/a ratios are considered. Table 2 shows the first five non-dimensional frequencies obtained by different methods. The results obtained in this study show good agreement compared with other researchers. The mode shapes of corresponding vibration modes are illustrated in Figure 3. In this case, the crack is clearly observed in mode 4 and mode 5.

Based on the non-dimensional frequencies in Table 1 and Table 2, one can see that the free vibration frequency decreases when the crack length increases. It means that the plate structure is weaken when the crack length increases, as expected.

Table 1. Non-dimensional frequency ϖ of a simply supported square plate with a central crack.

c/a	Ref. Results	Mode 1	Mode 2	Mode 3	Mode 4	Mode 5
0.0	Analytical [17]	19.739	49.348	49.348	78.957	98.696
	DDM [18]	19.740	49.350	49.350	78.960	98.700
	XFEM [19]	19.739	49.348	49.348	78.955	98.698
	This study	19.741	49.310	49.310	79.015	98.374
0.2	Analytical [17]	19.305	49.170	49.328	78.957	93.959
	DDM [18]	19.380	49.160	49.310	78.810	94.690
	XFEM [19]	19.305	49.181	49.324	78.945	93.893
	This study	19.407	49.261	49.322	79.004	94.906
0.4	Analytical [17]	18.279	46.624	49.032	78.602	85.510
	DDM [18]	18.440	46.440	49.040	78.390	86.710
	XFEM [19]	18.278	46.635	49.032	78.600	85.450
	This study	18.461	47.332	49.040	78.777	86.747
0.5	Analytical [17]	17.706	43.031	48.697	77.733	82.155
	DDM [18]	17.850	42.820	48.720	77.440	83.010
	XFEM [19]	17.707	43.042	48.685	77.710	82.108
	This study	17.898	44.789	48.731	78.243	83.192
0.6	Analytical [17]	17.193	37.978	48.223	75.581	79.588
	DDM [18]	17.330	37.750	48.260	75.230	80.320
	XFEM [19]	17.180	37.987	48.214	75.579	79.556
	This study	17.349	39.396	48.288	76.346	80.357
0.8	Analytical [17]	16.403	27.773	47.256	65.732	76.371
	DDM [18]	16.470	27.430	47.270	65.190	76.600
	XFEM [19]	16.406	27.753	47.201	65.715	76.351
	This study	16.506	28.823	47.285	67.195	76.761

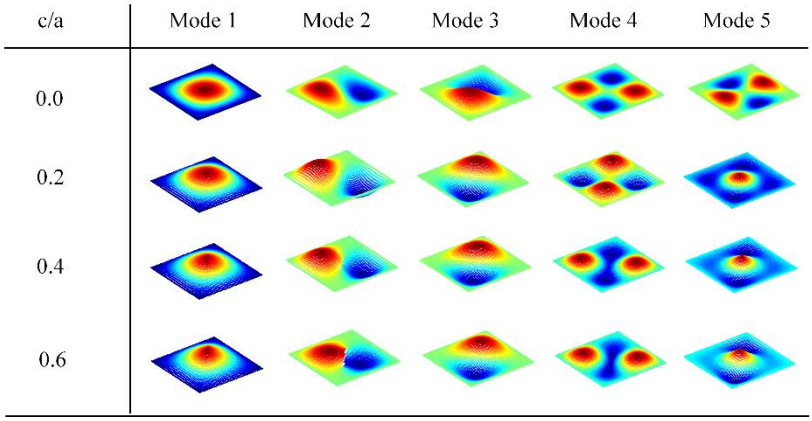

Figure 2. Mode shapes of five lowest modes of a square plate containing a central crack.

Table 2. Non-dimensional frequency ϖ of a simply supported rectangular plate with a central crack.

c/a	Ref. Results	Mode 1	Mode 2	Mode 3	Mode 4	Mode 5
0.2	XCS-DSG3 [20]	45.241	78.721	125.899	162.895	197.403
	XFEM [19]	45.724	78.790	125.679	163.533	197.274
	This study	46.330	78.884	126.244	164.935	197.240
0.4	XCS-DSG3 [20]	38.215	76.525	124.472	110.668	190.693
	XFEM [19]	38.576	76.793	124.099	109.488	191.101
	This study	39.328	77.155	124.316	116.282	192.972
0.5	XCS-DSG3 [20]	34.781	74.091	124.281	82.471	172.227
	XFEM [19]	35.257	74.575	124.036	82.667	173.490
	This study	35.783	74.987	124.161	86.239	177.492
0.6	XCS-DSG3 [20]	32.305	71.656	123.531	65.932	147.312
	XFEM [19]	32.476	71.809	123.350	64.707	145.595
	This study	32.898	72.280	123.598	66.978	150.069
0.8	XCS-DSG3 [20]	28.670	66.574	119.701	44.74	102.067
	XFEM [19]	28.750	66.629	119.424	43.858	100.114
	This study	29.050	67.055	119.759	44.997	102.790

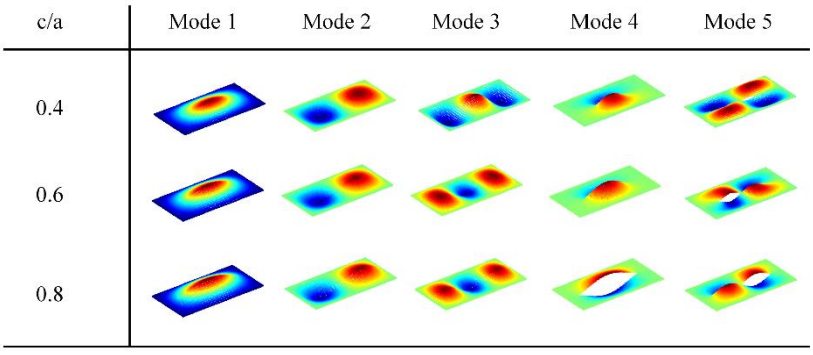

Figure 3. Mode shapes of five lowest modes of a rectangular plate containing a central crack.

3.2. Simply supported plate containing a side crack

The geometry of the two cases in this example is shown in Figure 4. The material properties in this example is Poisson's ratio $\nu = 0.3$. The non-dimensional frequency parameter ϖ is also used for comparison with other studies. In the case of square plate, the ratio of thickness to length $t/a = 0.001$ is used. The plate is discretized into a set of 50×50 nodes. The boundary condition is SSSS. Various c/a ratios are considered. Table 3 presents the first five non-dimensional frequencies, the results from XRPIM agree well with other methods. Figure 5 shows the mode shape of five vibration modes. Mode 1 is similar to the square plate with a central crack, while other modes are different. In this example, the crack is clearly observed.

In the second case, a ratio of $t/a = 0.001$ is used, the plate is discretized into 80×40 nodes and the boundary condition is SSSS. Various c/a ratios are considered. Table 4 shows the first five non-dimensional frequencies, the results in this study show good agreement compared with other researchers. The mode shapes of corresponding vibration modes are illustrated in Figure 6.

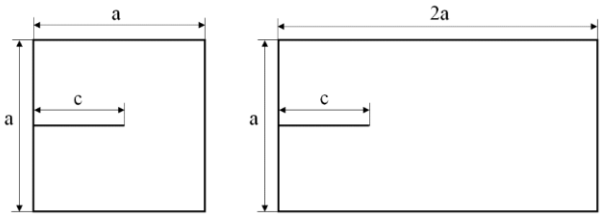

Figure 4. Geometry of square plate and rectangular plate with a side crack.

Table 3. Non-dimensional frequency parameter ϖ of a simply supported square plate with a side crack.

c/a	Ref. Results	Mode 1	Mode 2	Mode 3	Mode 4	Mode 5
0.2	XCS-DSG3 [20]	19.679	49.229	49.353	78.851	98.133
	Ritz method [21]	19.700	49.190	49.330	78.780	97.880
	This study	19.718	49.217	49.357	79.103	97.894
0.4	XCS-DSG3 [20]	19.175	47.774	48.305	71.571	92.451
	Ritz method [21]	19.200	47.800	48.240	71.270	92.230
	This study	19.259	48.228	48.298	72.955	92.749
0.5	XFEM [19]	18.646	44.213	47.916	65.789	88.063
	Ritz method [21]	18.650	43.420	47.920	64.400	88.080
	This study	18.706	44.594	47.942	65.452	88.895
0.6	XFEM [19]	17.956	37.693	47.862	63.282	83.753
	Ritz method [21]	17.960	36.450	47.860	62.240	83.780
	This study	18.050	37.628	47.849	62.401	84.397
0.8	XCS-DSG3 [20]	16.616	25.245	47.464	60.705	77.469
	XFEM [19]	16.662	26.226	47.446	61.774	77.378
	This study	16.732	25.706	47.433	61.039	77.752

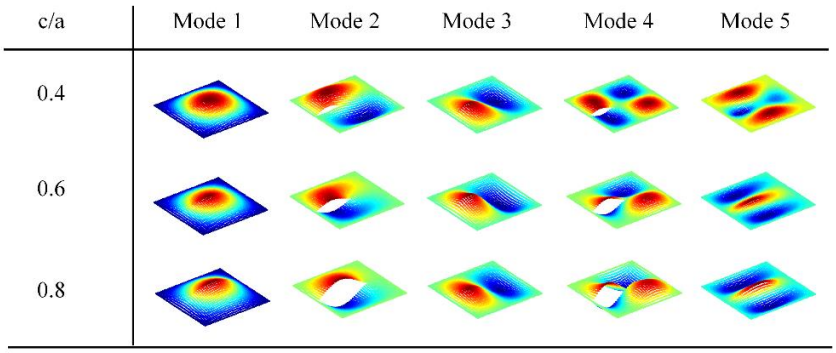

Figure 5. Mode shapes of five lowest modes of a square plate with a side crack.

Similar to the first example, it is observed that the free vibration frequency decreases when the crack length increases. It means that the plate structure is weaken when the crack length increases, as expected.

Table 4. Non-dimensional frequency ϖ of a simply supported rectangular plate with a side crack.

c/a	Ref. Results	Mode 1	Mode 2	Mode 3	Mode 4	Mode 5
0.2	Analytical [17]	48.953	77.871	126.578	167.092	194.036
	DDM [18]	48.050	78.080	126.900	167.200	194.700
	This study	49.032	78.060	126.912	167.168	195.234
0.4	Analytical [17]	44.512	73.282	124.456	100.078	173.754
	DDM [18]	45.400	73.820	124.500	104.700	173.700
	This study	44.823	73.464	124.609	103.214	173.624
0.5	Analytical [17]	40.367	72.788	123.419	73.627	168.573
	Ritz method [21]	40.350	72.780	123.400	73.630	168.900
	This study	40.761	72.831	123.720	76.132	170.320
0.6	XCS-DSG3 [20]	35.773	72.456	121.531	57.714	142.139
	DDM [18]	37.440	72.620	121.000	59.310	145.800
	This study	36.554	72.646	121.650	58.921	145.120
0.8	DDM [18]	30.500	68.820	120.300	40.020	95.790
	XFEM [19]	29.874	68.173	120.157	41.078	96.537
	This study	30.110	68.499	120.397	40.126	96.166

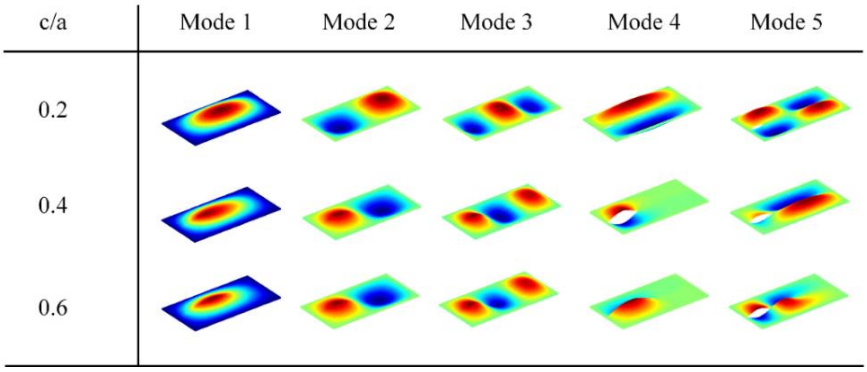

Figure 6. Mode shapes of five lowest modes of a rectangular plate with a side crack.

3.3. Square plate with a oblique crack

In this example, square plates with a central oblique crack and a side oblique crack are investigated. The geometry is shown in Figure 7.

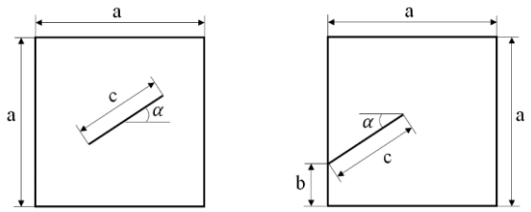

Figure 7. Geometry of square plate with a central oblique crack and a side oblique crack.

Table 5. Non-dimensional frequency ϖ of a simply supported square plate with a central oblique crack.

	c/a	Ref. Results	Mode 1	Mode 2	Mode 3	Mode 4	Mode 5
15	0.2	XCS-DSG3 [20]	19.278	49.177	49.378	78.930	94.376
		Ritz method [21]	19.330	49.180	49.320	78.790	94.390
		This study	19.427	49.253	49.320	78.893	95.285
	0.4	XCS-DSG3 [20]	18.224	46.157	48.995	77.446	87.229
		Ritz method [21]	18.270	46.600	49.000	77.590	87.040
		This study	18.571	48.059	49.074	78.035	88.770
	0.6	XCS-DSG3 [20]	17.061	37.604	48.049	73.622	82.312
		Ritz method [21]	17.100	37.960	48.060	74.030	82.190
		This study	17.524	44.575	48.275	75.373	84.072
30	0.2	XCS-DSG3 [20]	19.338	49.132	49.372	78.703	95.459
		Ritz method [21]	19.320	49.170	49.320	78.490	94.860
		This study	19.417	49.264	49.317	78.714	95.593
	0.4	XCS-DSG3 [20]	18.257	46.307	48.947	76.359	89.866
		Ritz method [21]	18.230	46.520	48.920	76.140	89.460
		This study	18.508	47.685	48.994	76.983	90.393
	0.6	XCS-DSG3 [20]	17.034	38.391	47.842	72.539	85.347
		Ritz method [21]	16.930	37.870	47.700	72.290	84.700
		This study	17.321	44.666	47.867	73.553	87.789
45	0.2	XCS-DSG3 [20]	19.262	49.056	49.335	78.511	95.172
		Ritz method [21]	19.320	49.170	49.320	78.350	95.120
		This study	19.373	49.242	49.313	78.574	95.375
	0.4	XCS-DSG3 [20]	18.396	46.626	48.949	76.364	91.287
		Ritz method [21]	18.210	46.480	48.890	75.560	90.570
		This study	18.404	47.348	48.943	76.233	90.956
	0.6	XCS-DSG3 [20]	16.916	37.318	47.564	71.953	83.596
		Ritz method [21]	16.840	37.850	47.510	71.600	84.580
		This study	17.159	41.492	47.740	72.545	89.890

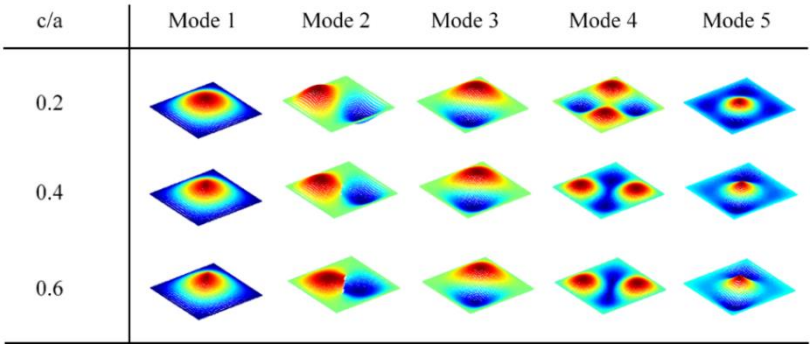

Figure 8. Mode shapes of five lowest modes of a square plate containing a central oblique crack.

Table 6. Non-dimensional frequency ϖ of a simply supported square plate with a side oblique crack.

	c/a	Ref. Results	Mode 1	Mode 2	Mode 3	Mode 4	Mode 5
15	0.2	XCS-DSG3 [20]	19.666	49.117	49.378	78.656	98.704
		Ritz method [21]	19.680	49.040	49.340	78.500	98.360
		This study	19.683	49.066	49.400	78.690	98.220
	0.4	XCS-DSG3 [20]	19.122	47.016	48.845	75.058	85.930
		Ritz method [21]	19.150	46.970	48.880	74.820	86.370
		This study	19.201	47.175	49.070	75.728	90.262
	0.6	XCS-DSG3 [20]	17.748	40.816	45.690	59.006	76.083
		Ritz method [21]	17.790	40.540	45.610	58.760	76.030
		This study	17.887	41.658	45.723	59.468	76.336
30	0.2	XCS-DSG3 [20]	19.641	49.117	49.379	78.848	98.406
		Ritz method [21]	19.640	49.030	49.350	78.690	98.030
		This study	19.656	49.035	49.422	78.898	97.911
	0.4	XCS-DSG3 [20]	19.064	47.436	48.863	75.212	87.651
		Ritz method [21]	19.070	47.390	48.890	75.120	87.140
		This study	19.108	47.422	49.111	76.193	89.954
	0.6	XCS-DSG3 [20]	17.729	39.266	46.292	60.717	77.834
		Ritz method [21]	17.780	39.990	46.380	60.770	77.660
		This study	17.839	41.298	46.291	61.241	78.039

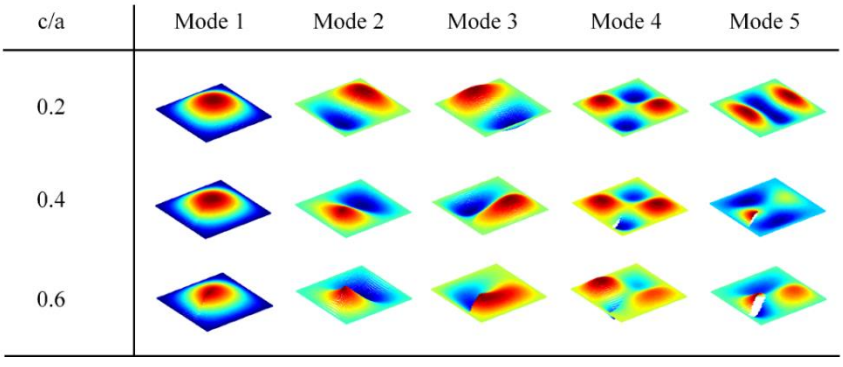

Figure 9. Mode shapes of five lowest mode of a square plate containing a side oblique crack.

Table 7. Non-dimensional frequency ϖ of a simply supported square plate with a central crack. The *c/a* ratio is 0.6 and $\alpha = 45^o$.

Ref. Results	Mode 1	Mode 2	Mode 3	Mode 4	Mode 5
XCS-DSG3 [20]	16.916	37.318	47.564	71.953	83.596
Ritz method [21]	16.840	37.850	47.510	71.600	84.580
Not aligned	17.159	41.492	47.740	72.545	89.890
Aligned	16.983	38.853	47.600	72.017	85.834

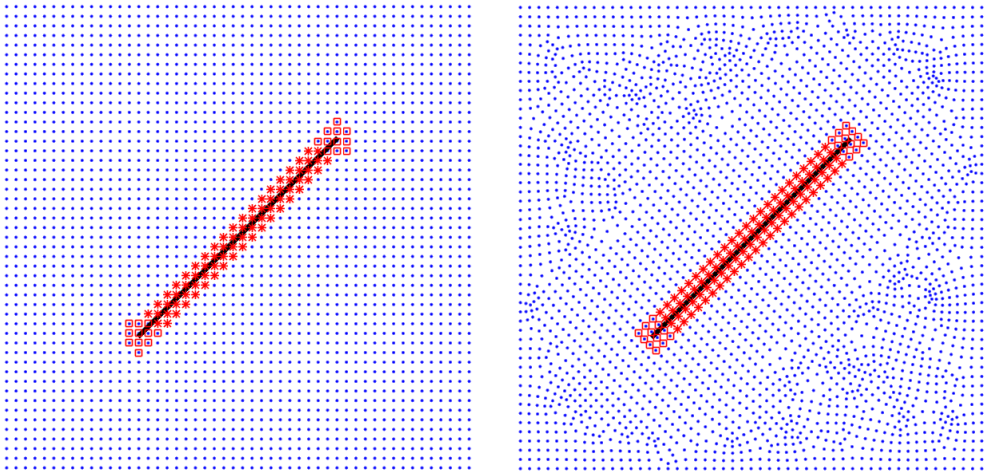

(a) (b)

Figure 10. Node distribution. (a) Not aligned with the crack, (b) Aligned with the crack.

The material properties in this example is Poisson's ratio $\nu = 0.3$. The non-dimensional frequency parameter ϖ is also used for comparison with other studies. In the case of central oblique crack, the ratio of thickness to length $t/a = 0.001$ is used. The plate is discretized into a set of 50×50 nodes. The boundary condition is SSSS. Various c/a ratios are considered. Table 5 presents the first five non-dimensional frequencies. Again, the results from XRPIM agree well with other methods. The mode shapes of $\alpha = 45^o$ are illustrated in Figure 8.

In the side oblique crack case, the relationship between a and b is $b = 0.25a$, a ratio of $t/a = 0.001$ is used. In this case, the plate is discretized into a set of 50×50 nodes and the boundary condition is SSSS. Various c/a ratios are considered. Table 6 shows the first five non-dimensional frequencies obtained by different methods. The results in this study show good agreement compared with other researchers. The mode shapes of $\alpha = 30^o$ are illustrated in Figure 9.

A significant deviation of non-dimensional frequency in this study is observed when the angle α increases. The cause of this deviation can be explained by the node distribution. The obtained results were computed in a uniform distribution of node (not aligned with the crack). Now, consider the node distribution aligned with the crack, as shown in Figure 10. The non-dimensional frequency of ratio *c/a* = 0.6 and $\alpha = 45^o$ are shown in Table 7. It is found that the results improve significantly when the node is distributed in alignment with the crack.

4. CONCLUSIONS

In this study, the XRPIM is used to investigate the free vibration behavior of Kirchhoff-Love plate. With the properties of RPIM formulation, the second derivative of shape functions in the Kirchhoff-Love plate theory is easily obtained. In the numerical example, a slight deviation is observed in the result of the oblique crack case. This is explained by the node distribution and can be corrected by using aligned-with-the-crack node distribution. However, the accuracy of the study is shown to be in good agreement with other researches. This is a promising method for analyzing thin plate structures, because of the low computational cost due to the use of only one DOF and simpler calculations for the Kirchhoff-Love plate compared with the Finite Element Method.

Acknowledgements. This research is funded by Vietnam National University Ho Chi Minh City (VNU-HCM) under grand number C2020-20-13.

Credit authorship contribution statement. Vay Siu Lo: Methodology, Investigation, Manuscript editor. Nha Thanh Nguyen and Minh Ngoc Nguyen: Gathering data, Checking the results, Manuscript review. Thien Tich Truong: Supervisor, Funding acquisition.

Declaration of competing interest. The authors declare that they have no known competing financial interests or personal relationships that could have appeared to influence the work reported in this paper.

REFERENCES

1. Moes N., Dolbow J. and Belytschko T. - A finite element method for crack growth without remeshing, Int. J. Numer. Methods Eng. **46** (1999) 131-150. https://doi.org/10.1002/(SICI)1097-0207(19990910)46:1<131::AID-NME726>3.0.CO;2-J
2. Dolbow J., Moes N. and Belytschko T. - Modeling fracture in mindlin-Reissner plates with the extended finite element method, Int. J. Solids Struct. **37** (2000) 7161-7183. https://doi.org/10.1016/S0020-7683(00)00194-3
3. Li J., Khodaei Z. S. and Aliabadi M. H. - Dynamic dual boundary element analysis for cracked Mindlin plates, Int. J. Solids Struct. **152–153** (2018) 248-260. https://doi.org/10.1016/j.ijsolstr.2018.06.033
4. Useche J. - Fracture dynamic analysis of cracked Reissner plates using the boundary element method, Int. J. Solids Struct. **191–192** (2020) 315-332. https://doi.org/10.1016/j.ijsolstr.2020.01.017
5. Lasry J., Renard Y. and Salaun M. - Stress intensity factors computation for bending plates with extended finite element method, Int. J. Numer. Methods Eng. **91** (2012) 909-928. https://doi.org/10.1002/nme.4292
6. Petyt M. - Introduction to Finite Element Vibration Analysis (2nd Edition), Cambridge, 2010.
7. Leitao Vitor M. A. - A meshless method for Kirchhoff plate bending problems, Int. J. Numer. Methods Eng. **52** (2001) 1107-1130. https://doi.org/10.1002/nme.244
8. Liu Y., Hon Y. C. and Liew K. M. - A meshfree Hermite-type radial point interpolation method for Kirchhoff plate problems, Int. J. Numer. Methods Eng. **66** (2006) 1153-1178. https://doi.org/10.1002/nme.1587

9. Nguyen N. T., Bui T. Q., Zhang C. and Truong T. T. - Crack growth modeling in elastic solids by the extended meshfree galerkin radial point interpolation method, Eng. Anal. Bound. Elem. **44** (2014) 87-97. https://doi.org/10.1016/j.enganabound.2014.04.021
10. Nguyen N. T., Bui T. Q. and Truong T. T. - Transient dynamic fracture analysis by an extended meshfree method with different crack-tip enrichments, Meccanica **52** (2017) 2363-2390. https://doi.org/10.1007/s11012-016-0589-6
11. Nguyen N. T., Bui T. Q., Nguyen M. N. and Truong T. T. - Meshfree thermomechanical crack growth simulations with new numerical integration scheme, Eng. Fract. Mech. **235** (2020) 107-121. https://doi.org/10.1016/j.engfracmech.2020.107121
12. Yang H. S. and Dong C. Y. - Adaptive extended isogeometric analysis based on PHT-splines for thin cracked plates and shells with Kirchhoff–Love theory, Appl. Math. Model. **76** (2019) 759-799. https://doi.org/10.1016/j.apm.2019.07.002
13. Liu G. R. and Chen X. L. - A mesh-free method for static and free vibration analyses of thin plates of complicated shape, J. Sound Vib. **241** (2001) 839-855. https://doi.org/10.1006/jsvi.2000.3330
14. Shojaee S., Izadpanah E., Valizadeh N. and Kiendl J. - Free vibration analysis of thin plates by using a NURBS-based isogeometric approach, Finite Elem. Anal. Des. **61** (2012) 23-34. https://doi.org/10.1016/j.finel.2012.06.005
15. Vu T. V., Nguyen N. H., Khosravifard A., Hematiyan M. R., Tanaka S. and Bui T. Q. - A simple FSDTbased meshfree method for analysis of functionally graded plates, Eng. Anal. Bound. Elem. **79** (2017) 1-12. https://doi.org/10.1016/j.enganabound.2017.03.002
16. Ferreira A. J. M. and Fantuzzi N. - Kirchhoff Plates. In: MATLAB Codes for Finite Element Analysis. Solid Mechanics and Its Applications, **157** (2020) Springer, Cham. https://doi.org/10.1007/978-3-030-47952-7_12
17. Stahl B. and Keer L. M. - Vibration and stability of cracked rectangular plates, Int. J. Solids Struct. **8** (1972) 69-91. https://doi.org/10.1016/0020-7683(72)90052-2
18. Liew K. M., Hung K. C. and Lim M. K. - A solution method for analysis of cracked plates under vibration, Eng. Fract. Mech. **48** (1994) 393-404. https://doi.org/10.1016/0013-7944(94)90130-9
19. Bachene M., Tiberkak R. and Rechak S. - Vibration analysis of cracked plates using the extended finite element method, Arch. Appl. Mech. **79** (2009) 249-262. https://doi.org/10.1007/s00419-008-0224-7
20. Nguyen-Thoi T., Rabczuk T., Lam-Phat T., Ho-Huu V. and Phung-Van P. - Free vibration analysis of cracked Mindlin plate using an extended cell-based smoothed discrete shear gap method (XCSDSG3), Theor. Appl. Fract. Mech. **72** (2014) 150-163. https://doi.org/10.1016/j.tafmec.2014.02.004
21. Huang C. S. and Leissa A. W. - Vibration analysis of rectangular plates with side cracks via the Ritz method, J. Sound Vib. **323** (2009) 974-988. https://doi.org/10.1016/j.jsv.2009.01.018